

Group IV Coordination Chemistry of a Tetradentate Redox-Active Ligand in Two Oxidation States

Karen J. Blackmore,^[a] Neetu Lal,^[a] Joseph W. Ziller,^[a] and Alan F. Heyduk^{*[a]}

Keywords: Redox-active ligands / Oxidation / N,O ligands / d⁰ metals / Macrocyclic ligands

The redox-active ligand *N,N'*-bis(3,5-di-*tert*-butyl-2-phenoxy)-1,2-phenylenediamide [N₂O₂^{red}]⁴⁻ reacts with group IV metal salts to form six- and seven-coordinate complexes [N₂O₂^{red}]ML_n (M = Ti, L = py, *n* = 2; M = Zr, Hf, L = thf, *n* = 3). The redox-active ligand occupies four equatorial coordination sites in these complexes. In the case of the zirconium and hafnium complexes, two axial solvent molecules coordinate to the metal center with a third solvent molecule coordinating in the equatorial plane. In the case of the smaller tita-

anium metal center, only two pyridine solvent molecules coordinate to the metal atom, leaving an open coordination site. All three complexes react with halogen oxidants to afford oxidative addition products [N₂O₂^{ox}]MCl₂L_n (M = Ti, *n* = 0; M = Zr, Hf, L = thf, *n* = 1), in which the redox-active ligand is oxidized by two electrons to the cyclohexadienediimine state.

(© Wiley-VCH Verlag GmbH & Co. KGaA, 69451 Weinheim, Germany, 2009)

Introduction

Redox-active ligands derived from catechol and related organic functionalities offer an intriguing way to approach multi-electron reactivity at a well-defined metal complex. For example, mid-transition metal catecholate and *ortho*-amidophenolate complexes act as catalysts for oxidation reactions with O₂.^[1] Zirconium(IV) ene-diamide complexes have been shown to react reversibly with O₂ to form zirconium(IV) bis(peroxide) complexes with concomitant oxidation of the ene-diamide ligands to the corresponding α -diimine oxidation state.^[2] Iridium amidophenolate complexes have been developed into molecular catalysts for hydrogen oxidation.^[3] Bis(imino)pyridine ligands have been found to be non-innocent in a variety of transition-metal complexes, and in one case this behaviour leads to unusual N₂ activation at a single iron center.^[4] In another multi-electron reaction, four-electron oxidation of a tantalum imido dimer with redox-active ligands resulted in the release of an organic diazene.^[5] We have been interested in developing further the coordination and reaction chemistry of redox-active ligands with early transition metals in order to bring late-transition-metal reactions, such as oxidative addition, reductive elimination, and group transfer, to electrophilic d⁰ metal complexes.

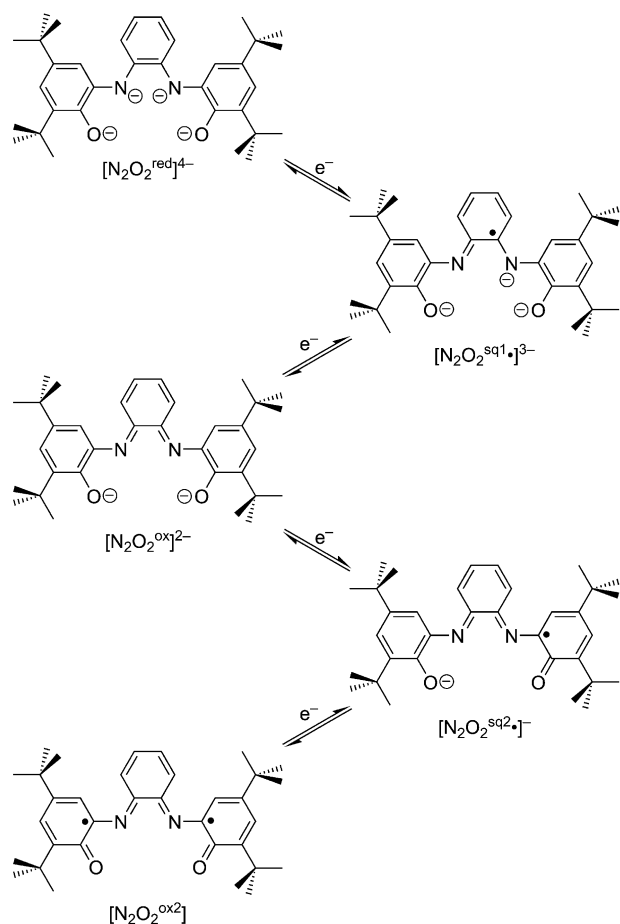
Oxidative addition and reductive elimination have been established as viable reaction pathways for group IV redox-active ligand complexes.^[6,7] Halogens were found to react

with Zr[ap]₂(thf)₂ {[ap]²⁻ = 4,6-di-*tert*-butyl-2-(*tert*-butyl-amido)phenolate}, resulting in ligand oxidation and halide addition to the metal atom. This reaction resembles a traditional oxidative addition sequence in that the halides add to the metal center; however, it is differentiated by the formal assignment of the reducing equivalents, which come from the amidophenolate ligands. Despite the success of this reaction with zirconium and hafnium, similar reactions with titanium were not successful due to ligand-exchange dynamics on the titanium center, which led to valence disproportionation and dissociation of the redox-active ligands. To overcome this limitation of bidentate, catecholate-type ligands, we became interested in the coordination and reaction chemistry of *N,N'*-bis(3,5-di-*tert*-butyl-2-phenoxy)-1,2-phenylenediamide ([N₂O₂^{red}]⁴⁻, Scheme 1), with electrophilic d⁰ metals.

The [N₂O₂^{red}]H₄ ligand was first reported by Wieghardt and co-workers, who studied complexes of the ligand with copper and zinc.^[8] Electrochemical and spectroscopic data showed that up to four electrons could be removed from the ligand platform with the two-electron oxidized form represented as the cyclohexadienediimine as shown in Scheme 1. The copper and zinc complexes serve as catalysts for the aerobic oxidation of primary alcohols under mild conditions. This reaction is remarkable, especially for zinc, which is a redox-inactive metal.

Whereas the [N₂O₂^{red}]⁴⁻ ligand can be viewed as a dimer of two bidentate *ortho*-amidophenolate ligands, it has several features that might add stability and increase reducing power relative to the simpler derivatives. The two amidophenolate groups of the [N₂O₂^{red}]⁴⁻ ligand are connected to *ortho* positions of a phenyl ring, resulting in a π system that is conjugated over three six-membered rings. Simple

[a] Department of Chemistry, University of California, Irvine, CA 92697, USA
Fax: 1-949-824-2210
E-mail: aheyduk@uci.edu



Scheme 1. Oxidation states of the $[\text{N}_2\text{O}_2]$ ligand platform as reported in ref.^[8]

extended Hückel calculations suggest that the HOMO of the $[\text{N}_2\text{O}_2^{\text{red}}]^{4-}$ ligand resides mainly on this linking phenylenediamine group, and as such two-electron oxidation would lead to a stable cyclohexadienediimine species as shown in Scheme 1. Furthermore, the $[\text{N}_2\text{O}_2^{\text{red}}]^{4-}$ ligand coordinates to transition metal atoms as a tetradentate chelate, which should engender stability to the metal complexes regardless of ligand oxidation state. This feature should stop disproportionation of ligand valence states and subsequent ligand dissociation events that have hampered further development of group IV metal chemistry with redox-active ligands. In this paper, we report the synthesis and characterization of titanium, zirconium, and hafnium complexes of the $[\text{N}_2\text{O}_2^{\text{red}}]^{4-}$ ligand, along with chlorine-based oxidation chemistry leading to the formation of oxidative addition products with the $[\text{N}_2\text{O}_2^{\text{ox}}]^{2-}$ ligand.^[9] This work is the first full report on the coordination chemistry of this tetradentate, redox-active ligand platform for electrophilic d^0 metals, and it established the structural and electronic features of the metal complexes for two ligand oxidation states.

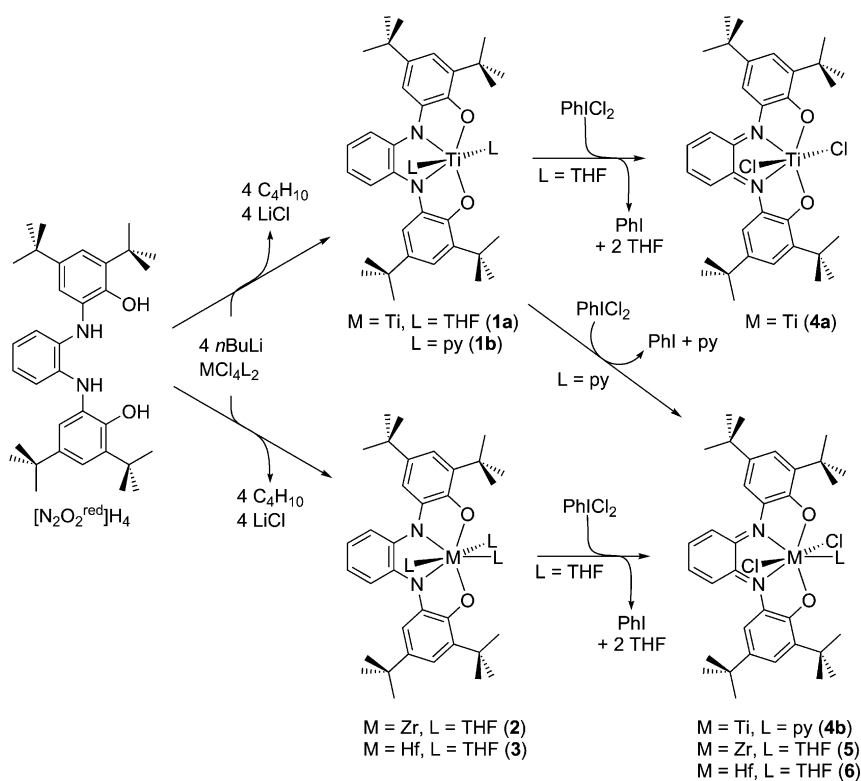
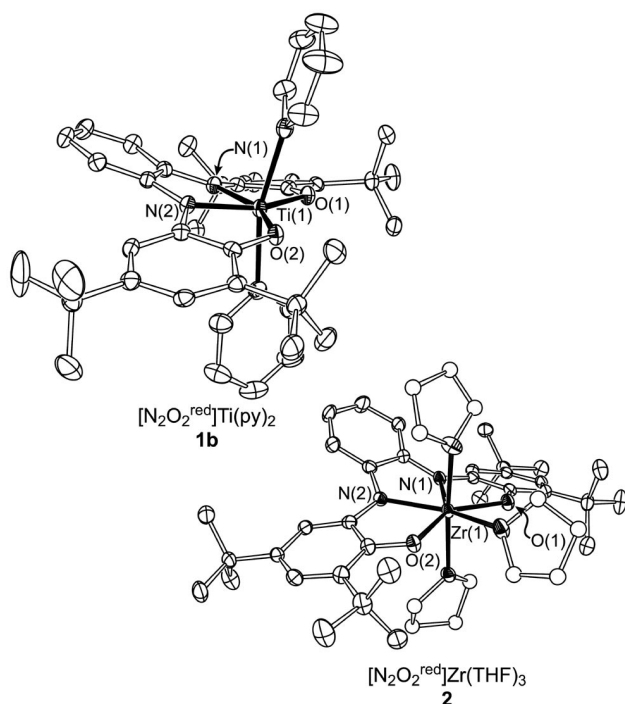
Results and Discussion

Reduced-Ligand Complexes

The condensation of 2 equiv. of 3,5-di-*tert*-butylcatechol with phenylenediamine affords the redox-active, tetradentate $[\text{N}_2\text{O}_2^{\text{red}}]\text{H}_4$ ligand as first reported by Wieghardt and co-workers.^[8] In their synthesis, the authors isolated $[\text{N}_2\text{O}_2^{\text{red}}]\text{H}_4$ as a pale yellow solid, which was analytically pure. In our hands, $[\text{N}_2\text{O}_2^{\text{red}}]\text{H}_4$ prepared in this way gave unreliable metallation results with group IV metals, and products often were contaminated with paramagnetic impurities that could not be separated from the desired products. As such, we have added a purification step to the synthesis of $[\text{N}_2\text{O}_2^{\text{red}}]\text{H}_4$. When the pale-yellow, crude product was dissolved in diethyl ether, it formed a yellow solution, which was filtered through a plug of silica gel. Following diethyl ether removal, the pale blue residue was washed with cold pentane to afford $[\text{N}_2\text{O}_2^{\text{red}}]\text{H}_4$ as a pure white powder. Purification of $[\text{N}_2\text{O}_2^{\text{red}}]\text{H}_4$ in this way only resulted in the loss of 1–2% of the crude material, but gave much more reliable syntheses of the following coordination complexes.

Metallation of $[\text{N}_2\text{O}_2^{\text{red}}]\text{H}_4$ with group IV metals was readily achieved by using solvent adducts of the metal tetrachloride salts as shown in Scheme 2. All four acidic protons of $[\text{N}_2\text{O}_2^{\text{red}}]\text{H}_4$ may be removed with *n*BuLi, providing an easy metathesis metallation route for the halide salts of titanium, zirconium, and hafnium. In the case of titanium, addition of solid $\text{TiCl}_4(\text{thf})_2$ to a cold diethyl ether solution of $[\text{N}_2\text{O}_2^{\text{red}}]\text{Li}_4$ resulted in a color change to deep red with concomitant precipitation of LiCl as a white solid. After filtration and solvent removal, the product, $[\text{N}_2\text{O}_2^{\text{red}}]\text{Ti}(\text{thf})_2$ (**1a**), was obtained as red crystals from pentane in modest yields. Similarly, the bis(pyridine) adduct, $[\text{N}_2\text{O}_2^{\text{red}}]\text{Ti}(\text{py})_2$ (**1b**), was isolated as purple crystals by using the $\text{TiCl}_4(\text{py})_2$ starting material. In the cases of zirconium and hafnium, reactions of $[\text{N}_2\text{O}_2^{\text{red}}]\text{Li}_4$ and $\text{MCl}_4(\text{thf})_2$ ($\text{M} = \text{Zr}, \text{Hf}$) gave $[\text{N}_2\text{O}_2^{\text{red}}]\text{Zr}(\text{thf})_3$ (**2**) and $[\text{N}_2\text{O}_2^{\text{red}}]\text{Hf}(\text{thf})_3$ (**3**), as yellow microcrystalline solids from diethyl ether.

X-ray crystallography was used to establish the coordination geometry of complexes **1–3**. As shown in Figure 1, titanium complex **1b** is a six-coordinate complex; selected bond lengths and angles can be found in Table 1. Complex **1b** is a severely distorted octahedron, owing to the constrained geometry imposed by the $[\text{N}_2\text{O}_2^{\text{red}}]^{4-}$ ligand. The sum of the three angles encompassed by the ligand is 233° , leaving a rather open site between the two oxygen atoms of the ligand [$\text{O}-\text{Ti}-\text{O}$ $126.95(8)^\circ$]. Whereas the titanium center and four heteroatom donors of the $[\text{N}_2\text{O}_2^{\text{red}}]^{4-}$ ligand are nearly coplanar, the rest of the ligand framework shows a distinct ruffle, which tilts the central phenylenediamine ring up and the two aminophenol rings down. The Ti–O and Ti–N bond lengths for the $[\text{N}_2\text{O}_2^{\text{red}}]^{4-}$ ligand are consistent with these groups coordinating as phenoxide and anilide, respectively. The coordination sphere of **1b** is completed by two axial pyridine molecules, which are bent towards the open section of the equatorial plane, resulting in an N–Ti–N angle of $164.70(9)^\circ$.

Scheme 2. Syntheses of redox-active ligand complexes $[\text{N}_2\text{O}_2^{\text{red}}]\text{ML}_n$ (**1–3**) and $[\text{N}_2\text{O}_2^{\text{ox}}]\text{MCl}_2\text{L}_n$ (**4–6**).Figure 1. ORTEP diagrams for $[\text{N}_2\text{O}_2^{\text{red}}]\text{Ti}(\text{py})_2$ (**1b**) and $[\text{N}_2\text{O}_2^{\text{red}}]\text{Zr}(\text{thf})_3$ (**2**). Ellipsoids are drawn at 50% probability. Hydrogen atoms and solvent molecules are excluded for clarity.

Zirconium and hafnium complexes, **2** and **3**, respectively, adopt a seven-coordinate geometry in the solid state. The structure of **2** has been reported previously,^[9] but for com-

Table 1. Selected bond lengths and angles for $[\text{N}_2\text{O}_2^{\text{ox}}]\text{TiCl}_2$ (**4a**) and $[\text{N}_2\text{O}_2^{\text{ox}}]\text{ZrCl}_2(\text{thf})$ (**5**).

	Bond lengths [Å]	
	$[\text{N}_2\text{O}_2^{\text{red}}]\text{Ti}(\text{py})_2$ (4b)	$[\text{N}_2\text{O}_2^{\text{ox}}]\text{TiCl}_2$ (4a)
Ti–O(1)	1.9275(18)	1.873(2)
Ti–O(2)	1.9185(18)	–
Ti–N(1)	2.002(2)	2.114(3)
Ti–N(2)	1.996(2)	–
Ti–Cl(1)	–	2.3580(12)
Ti–N(3) ^[a]	2.217(2)	–
Ti–N(4) ^[a]	2.220(2)	–
	Bond angles [°]	
	$[\text{N}_2\text{O}_2^{\text{red}}]\text{Ti}(\text{py})_2$ (4b)	$[\text{N}_2\text{O}_2^{\text{ox}}]\text{TiCl}_2$ (4a)
O(1)–Ti–N(1)	78.68(8)	79.01(11)
O(2)–Ti–N(2)	78.86(8)	–
N(1)–Ti–N(2)	75.66(9)	75.83(16) ^[b]
O(1)–Ti–O(2)	126.95(8)	126.17(15) ^[b]
N(3)–Ti–N(4) ^[a]	164.70(9)	–
Cl(1)–Ti–Cl(1)′	–	174.87(6)

[a] N(3) and N(4) are pyridine nitrogen atoms. [b] Angle between symmetry-equivalent N(1) and O(1) atoms, respectively.

parison an ORTEP plot is shown in Figure 1 alongside the titanium congener. The coordination geometry of complex **2** is similar to that of **1b**; however, a third solvent molecule is coordinated in the equatorial plane, resulting in a pentagonal-bipyramidal structure. By virtue of the larger zirconium radius, the $[\text{N}_2\text{O}_2^{\text{red}}]^{4-}$ ligand occupies a smaller fraction of the equatorial plane around the zirconium center, which opens the O–Zr–O angle by 20° to 143° in **2**, allowing the coordination of a third thf molecule. As such the angle

between the axial thf molecules opens to 175° reflecting the more crowded equatorial plane. The Zr–O bond lengths to the coordinated thf molecule provide further evidence of steric crowding in the equatorial plane of **2** [Zr–O_{axial} 2.235(4) and 2.252(4) Å; Zr–O_{equatorial} 2.369(4) Å], suggesting that the third thf ligand is weakly bound. All other Zr–O and Zr–N bond lengths are in the expected range of phenoxides and anilides bound to a zirconium atom. In the case of hafnium derivative **3**, only weakly diffracting crystals were obtained after repeated crystallization attempts. As such the diffraction data for **3** were of poor quality. While this data could confirm a seven-coordinate geometry analogous to zirconium complex **2**, it was not suitable for examination of detailed structural features.

Solution characterization data for **1–3** from NMR spectroscopy was consistent with the solid-state structural data. The ¹H NMR spectra of titanium derivatives **1a** and **1b** in C₆D₆ are identical, save for the resonances associated with the coordinated thf and pyridine ligands, respectively. Notably, the four protons of the *ortho*-phenylenediamide ring in **1a** and **1b** appear as two doublet-of-doublet resonances at δ = 6.75 and 7.30 ppm, whereas the aromatic protons of the *ortho*-amidophenolate rings appear as two doublets at δ = 7.06 and 7.35 ppm. Two resonances are observed for the coordinated thf molecules of **1a** at δ = 1.26 and 4.29 ppm, which are shifted by less than 1 ppm from those of free thf in C₆D₆; similarly small shifts are observed for the proton resonances of the coordinated pyridine molecule in **1b**. Overall, the NMR spectroscopic data for complexes **1a** and **1b** is consistent with approximate C_{2v} symmetry in solution.

Zirconium and hafnium derivatives **2** and **3** gave analogous NMR spectra, which were nearly superimposable. Despite the increase in coordination number to seven observed for **2** and **3**, the ¹H NMR resonances for the *ortho*-phenylenediamide ring shift further downfield to δ = 7.00 and 7.88 ppm, suggesting a more electrophilic metal center. Only two ¹H NMR resonances are observed for the coordinated thf molecules; moreover, whereas the signal of the protons on the β-carbon atom are shifted upfield to δ = 0.83 ppm, those protons on the α-carbon atom resonate close to the frequency of free thf at δ = 3.79 ppm. Similarly, only two ¹³C NMR resonances were observed for the coordinated thf molecules in **3**, whereas no signals attributable to thf were observed in the ¹³C NMR spectrum of **2**. These NMR results are consistent with rapid exchange of the axial and equatorial thf ligands of **2** and **3** on the NMR time-scale, which probably proceeds through dissociation of a thf ligand. Further evidence for such an exchange process was obtained for NMR spectra in [D₈]thf, which showed instant exchange of coordinated [H₈]thf for the [D₈]thf.

The electronic spectra of complexes **1–3** are remarkably similar, even though their solid-state colors vary from nearly colorless for hafnium complex **3** to purple for titanium complex **1b**. The UV/Vis absorbance spectra of **1–3** are dominated by an intense UV absorbance at 330 nm (ε ≈ 10⁴ M⁻¹ cm⁻¹), analogous to that reported for the copper(II) dianion, {[N₂O₂^{red}]Cu^{II}}²⁻.^[8] Titanium derivatives **1a** and **1b** both show a shoulder at 380 nm, which tails into the

visible region of the spectrum. The titanium–pyridine adduct **1b** shows a further absorbance at 530 nm (ε = 3 × 10³ M⁻¹ cm⁻¹), consistent with ligand-to-ligand charge-transfer transitions observed in other group IV pyridine complexes. This absorbance likely leads to the purple colour observed for solid samples of **1b**.

Oxidized-Ligand Complexes

To evaluate the ability of the [N₂O₂^{red}]⁴⁻ ligand to support redox reactivity at d⁰ transition metals, chlorine-based oxidations were carried out with complexes **1–3** (Scheme 2). Previous attempts to carry out halogen oxidation reactions with titanium complexes of redox-active ligands resulted in messy ligand disproportionation reactions.^[10] We hoped that the tetradentate nature of the [N₂O₂^{red}]⁴⁻ ligand would prevent disproportionation and dissociation of the redox-active ligand upon halogen oxidative addition. Thus, the addition of the chlorine surrogate PhICl₂ to a solution of **1a** in diethyl ether resulted in a rapid color change to dark green. Storage of the reaction mixture at -35 °C overnight resulted in the precipitation of dark green crystals identified as [N₂O₂^{ox}]TiCl₂ (**4a**) in modest yields. A similar reaction between PhICl₂ and pyridine adduct **1b** afforded the related complex [N₂O₂^{ox}]TiCl₂(py) (**4b**). Analogous reactivity was observed for zirconium and hafnium complexes **2** and **3**, which afforded [N₂O₂^{ox}]ZrCl₂(thf) (**5**) and [N₂O₂^{ox}]HfCl₂(thf) (**6**), respectively, upon treatment with PhICl₂. Attempts to generate odd-electron species through the addition of 0.5 or 1.5 equiv. of PhICl₂ resulted only in reduced yields of the two-electron oxidized products **4–6**.

The solid-state structures of complexes **4a** and **5** were interrogated by single-crystal X-ray diffraction methods. Figure 2 gives ORTEP diagrams derived from the X-ray diffraction data for complexes **4a** and **5**; selected metrical parameters for **4a** are shown in Table 1. The coordination environment in **4a** is similar to that observed for **1a** in that the titanium center is six-coordinate with the redox-active ligand occupying four equatorial positions. In the case of **4a**, however, chlorido ligands from the halogen oxidation occupy the metal atom's axial positions. The zirconium oxidation product **5** is structurally analogous to the reduced complex **2**, except for the coordination of axial chlorido ligands in the place of thf molecules. As observed in **2**, the coordination of a thf ligand in the equatorial plane of **5** creates a crowded environment, which is reflected in a long Zr–O(thf) bond of 2.265(5) Å.

X-ray diffraction studies also provide unequivocal evidence for ligand oxidation accompanying halide addition to the titanium center in complex **4a**.^[11] The Ti–Cl bond length in **4a** is consistent with a chloride ion bound to a titanium(IV) metal center. As shown in Table 1 the ligand–titanium angles for the redox-active ligand in **4a** are nearly identical to the values observed in **1b**; however, the Ti–O and Ti–N bond lengths are significantly different. A small contraction is observed in the Ti–O bond lengths, whereas an elongation of over 0.1 Å is observed in the Ti–N bond

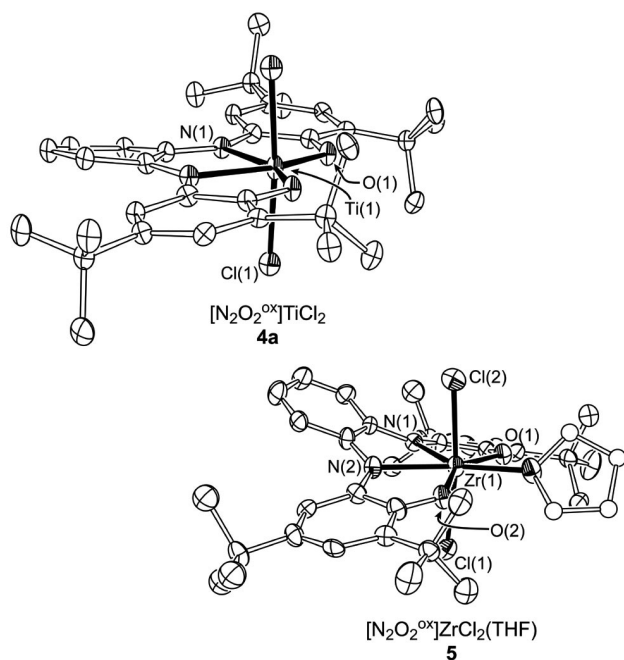


Figure 2. ORTEP diagrams for $[\text{N}_2\text{O}_2^{\text{ox}}]\text{TiCl}_2$ (**4a**) and $[\text{N}_2\text{O}_2^{\text{ox}}]\text{-ZrCl}_2(\text{thf})$ (**5**). Ellipsoids are drawn at 50% probability. Hydrogen atoms and solvent molecules are excluded for clarity.

lengths of **4a**. These bond length changes are consistent with the nitrogen atoms acting as neutral imine donor in **4a**, and the oxygen atoms acting as anionic phenolate donors. Figure 3 compares redox-active-ligand bond lengths from the structures of **1b** and **4a**. The C–C bond lengths within the redox-active ligand of **1b** fall in the 1.39–1.41 Å range (Figure 3a), as expected for aromatic phenyl rings. In contrast, the central, six-membered ring of the redox-active ligand in **4a** (Figure 3b) shows C–C bond lengths that alternate between 1.35 Å and 1.44 Å, indicative of a non-aromatic, cyclohexadiene ring. Whereas some C–C bond-length variation is also observed in the *ortho*-amidophenolate rings of **4a**, the difference is much smaller and within the error of the experimental measurement. The crystallographic bond lengths observed in the structure of **4b** suggest that the best resonance structure for $[\text{N}_2\text{O}_2^{\text{ox}}]\text{TiCl}_2$ is that depicted in Figure 3, namely a cyclohexadienediimine. Similar metrical parameters are observed in the crystal structure of **5**, consistent with the formulation $[\text{N}_2\text{O}_2^{\text{ox}}]\text{-ZrCl}_2(\text{thf})$.

NMR spectra of **4–6** show further evidence of ligand oxidation. The ^1H NMR spectrum of **4a** showed changes diagnostic for ligand oxidation in the aromatic portion of the spectrum. Notably, one proton resonance for the cyclohexadienediimine ring shifts upfield by 0.2 ppm to $\delta = 6.5$ ppm, whereas the other proton resonance shifts downfield by 0.3 ppm to $\delta = 7.6$ ppm. In the case of the aminophenolate rings, the two aromatic resonances of **4a** shift downfield by 0.3–0.5 ppm relative to the same resonances in **1a**. The ^1H and ^{13}C NMR spectra of **4b** are virtually the same as those observed for **4a**, with the exception of resonances for the coordinated pyridine molecule. In the

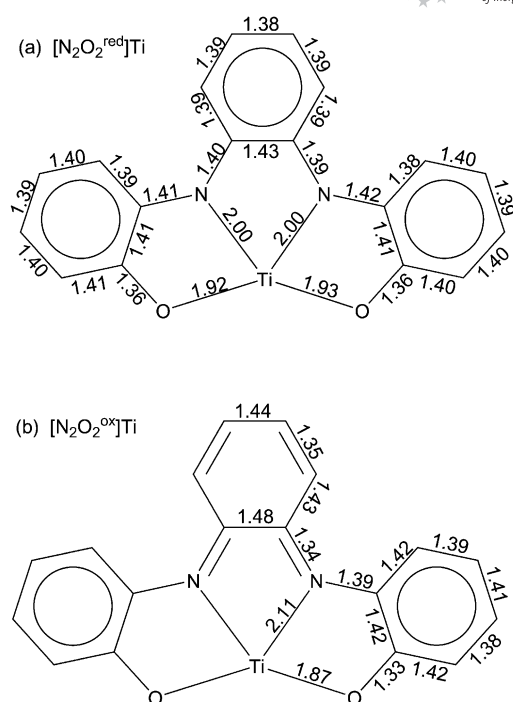


Figure 3. Redox-active-ligand bond lengths from the X-ray crystal structures of (a) $[\text{N}_2\text{O}_2^{\text{red}}]\text{Ti}(\text{py})_2$ (**1b**) and (b) $[\text{N}_2\text{O}_2^{\text{ox}}]\text{TiCl}_2$ (**4a**). *tert*-Butyl groups, chlorido ligands, and coordinated solvent molecules are omitted for clarity.

room-temperature ^1H NMR spectrum the pyridine protons appeared as sharp triplets and singlets, suggesting that the complex is seven-coordinate and static on the NMR timescale.

In the case of zirconium dichloride complex **5** and hafnium dichloride complex **6**, the ^1H NMR spectra are indistinguishable, except for the peak shape of the resonances for the coordinated thf molecule. In hafnium complex **6**, the thf protons resonate as relatively sharp singlets at $\delta = 1.59$ and 4.75 ppm; in zirconium complex **5**, the thf proton resonances are broadened significantly, suggesting that exchange is occurring on the NMR timescale. This contention is further supported by the ^{13}C NMR spectroscopic data. The thf carbon resonances were readily observed at $\delta = 25.3$ and 74.2 ppm for **6**, whereas the same resonances for **5** were broadened into the spectral baseline.

Distinct changes in color accompanied the chlorine oxidations of **1–3**, prompting an investigation of the UV/Vis absorbance spectra of products **4–6**. Figure 4 shows the room-temperature UV/Vis absorbance spectra of complexes **4–6** in thf. The spectra for zirconium complex **5** and hafnium complex **6** are dominated by an intense absorbance near 937 nm ($\epsilon = 2.0 \times 10^4 \text{ M}^{-1} \text{ cm}^{-1}$), with a high-energy shoulder near 750 nm, resulting in the observed dark-green color for the oxidized complexes. These absorbances are consistent with ligand-based, $\pi \rightarrow \pi^*$ transitions. The low-energy absorbance for titanium complexes **4a** and **4b** (not shown) is slightly redshifted ($\lambda_{\text{max}} = 947 \text{ nm}$; $\epsilon = 1.3 \times 10^4 \text{ M}^{-1} \text{ cm}^{-1}$) relative to the zirconium and hafnium derivatives. Complexes **4a** and **4b** also show a strong transi-

tion to higher energy at 427 nm ($\epsilon = 1.55 \times 10^4 \text{ M}^{-1} \text{ cm}^{-1}$). A similar transition is observed in the zirconium and hafnium complexes, albeit with a much lower intensity ($\lambda_{\text{max}} = 460 \text{ nm}$, $\epsilon = 3 \times 10^3 \text{ M}^{-1} \text{ cm}^{-1}$).

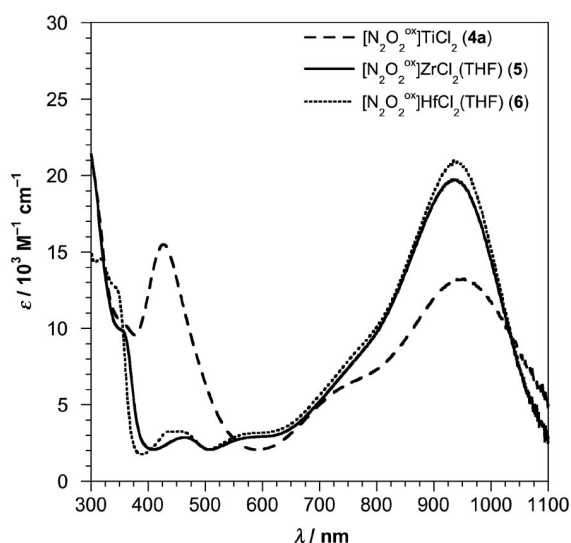
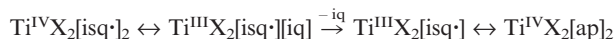


Figure 4. UV/Vis absorbance spectra for $[\text{N}_2\text{O}_2^{\text{ox}}]\text{TiCl}_2$ (**4a**), $[\text{N}_2\text{O}_2^{\text{ox}}]\text{ZrCl}_2(\text{thf})$ (**5**), and $[\text{N}_2\text{O}_2^{\text{ox}}]\text{HfCl}_2(\text{thf})$ (**6**) in thf solution at room temperature.

Conclusions

The $[\text{N}_2\text{O}_2^{\text{red}}]^{4-}/[\text{N}_2\text{O}_2^{\text{ox}}]^{2-}$ ligand platform provides a robust framework for two-electron chemistry at d^0 metal centers. Previous efforts in our research group focused on the redox chemistry of zirconium with bidentate *ortho*-amido-phenolate ligands ($[\text{ap}]^{2-}$). Whereas oxidative addition and reductive elimination chemistry were realized for d^0 metal centers, the chemistry was always dominated by the imino-semiquinone ($[\text{isq}\cdot]^-$) oxidation state of the ligand, which shows surprising stability, even in its neutral, protonated form. Whereas oxidized complexes of the form $\text{ZrX}_2(\text{isq}\cdot)_2$ could be obtained by halogen oxidative addition reactions, similar species were not accessible for titanium derivatives, where a titanium(III) oxidation state is viable.^[10] In the titanium case, a valence tautomerization^[12] could give Ti^{III} and an iminoquinone ligand (iq), which would readily dissociate from the d^0 metal center. In contrast, the tetradentate $[\text{N}_2\text{O}_2^{\text{ox}}]^{2-}$ ligand cannot dissociate, even if a valence tautomerization is established.



Given the well-defined electrochemistry of metal complexes of the $[\text{N}_2\text{O}_2^{\text{ox}}]^{2-}$ ligand (Scheme 1),^[8] it was surprising that one- and three-electron oxidation products could not be isolated for titanium, zirconium, and hafnium. When 0.5 equiv. of PhICl_2 or 1.5 equiv. of PhICl_2 was added to complexes **1–3**, only a reduced yield of the two-electron products **4–6** could be isolated. In the case of the addition of 0.5 equiv. of PhICl_2 to zirconium complex **2**, the major

zirconium species identified for the reaction were dichloride **5** and the unreacted zirconium starting material. Hence, the putative one-electron product, $[\text{N}_2\text{O}_2^{\text{sq}1}\cdot]\text{ZrCl}_2$, could not be isolated (although this does not preclude its formation either as an intermediate or as a minor product).

In addition to the increased stability of metal complexes of the $[\text{N}_2\text{O}_2^{\text{ox}}]^{2-}$ ligand, the geometry enforced by the ligand platform may have important implications for both stoichiometric and catalytic reactions. Superficially, the $[\text{N}_2\text{O}_2]$ ligand platform resembles a salen-type ligand. In the case of the two-electron oxidized form, $[\text{N}_2\text{O}_2^{\text{ox}}]^{2-}$, this resemblance extends to the ligand being isoelectronic with salen ligands, as $[\text{N}_2\text{O}_2^{\text{ox}}]^{2-}$ has two neutral imine donors and two anionic phenoxide donors. Whereas salen-type ligands typically form six-coordinate complexes with titanium(IV),^[13] seven-coordinate complexes are often observed for complexes of the larger metals zirconium and hafnium.^[14] In the $[\text{N}_2\text{O}_2]$ ligand platform, the formation of three five-membered chelates upon metal coordination results in access to seven-coordinate geometries for all three metal ions. In the case of zirconium derivatives **2** and **5**, these seven-coordinate species are fluxional on the NMR timescale. Rapid exchange of the equatorial ligand in these seven-coordinate complexes provides an entry point for the addition of substrates to the metal center,^[9] and such additions may be exploited for stoichiometric and catalytic atom- and group-transfer studies.

Experimental Section

General Experimental Considerations: The complexes described below are extremely air- and moisture-sensitive. Except where noted, all manipulations were carried out under argon or nitrogen gas by using standard Schlenk, vacuum-line, and glovebox techniques. High-purity solvents were first sparged with argon and then passed through activated alumina and Q5 columns to remove water and oxygen, respectively. The metal salts TiCl_4 , ZrCl_4 , and HfCl_4 (Alfa-Aesar) and 3,5-di-*tert*-butylcatechol (Acros) were used as received. *ortho*-Phenylenediamine (Alfa-Aesar) was purified by vacuum sublimation. The starting materials $\text{TiCl}_4(\text{thf})_2$, $\text{ZrCl}_4(\text{thf})_2$, $\text{HfCl}_4(\text{thf})_2$, and PhICl_2 were synthesized according to published procedures.^[15,16] All complexes were characterized by ^1H and ^{13}C NMR spectroscopy, IR spectroscopy, and elemental analysis. NMR spectra were collected with Bruker Avance 500 or 600 MHz spectrometers in either $[\text{D}_6]\text{benzene}$ or $[\text{D}_8]\text{thf}$ solvents that were degassed by several freeze-pump-thaw cycles, dried with sodium benzophenone ketyl radical, and vacuum-distilled before use. ^1H and ^{13}C NMR spectra were referenced to TMS by using the residual ^1H and natural abundance ^{13}C impurities of the solvent. All chemical shifts are reported by using the standard δ notation in parts per million. IR spectra were recorded with a Perkin-Elmer Spectrum One spectrophotometer as KBr pellets. Elemental analyses were provided by Desert Analytics or Schwarzkopf Microanalytical Laboratory, Inc.

***N,N'*-Bis(3,5-di-*tert*-butyl-2-hydroxyphenyl)-1,2-phenylenediamine ($[\text{N}_2\text{O}_2^{\text{red}}]\text{H}_4$):** The $[\text{N}_2\text{O}_2^{\text{red}}]\text{H}_4$ ligand was prepared according to the procedure reported by Wieghardt and co-workers with minor modifications that lead to a higher-purity product.^[8] Freshly sublimed *ortho*-phenylenediamine (2.06 g, 19 mmol), NEt_3 (0.4 mL), and 3,5-di-*tert*-butylcatechol (8.9 g, 38 mmol) were dissolved in

heptane (150 mL). The solution was stirred open to air for 4 d, during which time a yellow precipitate formed (the solution was greenish-brown). The yellow solid was collected, dissolved in diethyl ether (30 mL), and filtered through a silica plug. The silica was washed with additional diethyl ether (150 mL), and all diethyl ether fractions were combined and taken to dryness in a rotovapor. The resulting blue residue was taken up in cold pentane and stirred, resulting in the precipitation of a white solid from the blue solution. The white solid was collected and washed with cold pentane until the washings were colorless. The overall yield was 4.3 g (44%) of analytically pure $[\text{N}_2\text{O}_2^{\text{red}}]\text{Hf}_4$. Analytical data for $[\text{N}_2\text{O}_2^{\text{red}}]\text{Hf}_4$ prepared by this procedure matched the data reported in the literature.

$[\text{N}_2\text{O}_2^{\text{red}}]\text{Ti}(\text{thf})_2$ (1a): In a 20-mL scintillation vial, a diethyl ether solution (10 mL) containing $[\text{N}_2\text{O}_2^{\text{red}}]\text{Li}_4$ {1.93 mmol; prepared in situ from $[\text{N}_2\text{O}_2^{\text{red}}]\text{H}_4$ (1.00 g) and 2.71 M *n*-butyllithium (2.86 mL)} was frozen in a liquid-nitrogen cold well. Immediately upon thawing, the $[\text{N}_2\text{O}_2^{\text{red}}]\text{Li}_4$ mixture was added to a stirred suspension of $\text{TiCl}_4(\text{thf})_2$ (0.46 g 1.93 mmol) in cold diethyl ether. The reaction mixture was warmed to 26 °C and stirred overnight to afford a dark-red solution and a white precipitate. The white solid was removed by filtration, and the solvent was stripped from the red mother liquor under reduced pressure. The resulting residue was triturated with pentane (3 × 10 mL) and then dissolved in a fourth aliquot of pentane, which was cooled to -35 °C overnight. Collection of the red crystals gave **4a** (0.78 g, 52% yield). $\text{C}_{42}\text{H}_{60}\text{N}_2\text{O}_4\text{Ti}$ (704.79): calcd. C 71.57, H 8.58, N 3.97; found C 72.01, H 8.39, N 3.42. ^1H NMR (600 MHz, C_6D_6): δ = 1.26 (s, 12 H, thf), 1.38 [s, 18 H, $\text{C}(\text{CH}_3)_3$], 1.51 [s, 18 H, $\text{C}(\text{CH}_3)_3$], 4.29 (s, 12 H, thf), 6.77 (dd, $^3J_{\text{HH}} = 6.0$ and 3.0 Hz, 2 H, aryl-H), 7.05 (d, $^3J_{\text{HH}} = 1.8$ Hz, 2 H, aryl-H), 7.28 (dd, $^3J_{\text{HH}} = 6.0$ and 3.0 Hz, 2 H, aryl-H), 7.31 (d, $^3J_{\text{HH}} = 1.8$ Hz, 2 H, aryl-H) ppm. ^{13}C NMR (150 MHz, C_6D_6): δ = 25.4 (thf), 30.1 [$\text{C}(\text{CH}_3)_3$], 32.2 [$\text{C}(\text{CH}_3)_3$], 34.8 (thf), 108.5 (aryl-C), 108.7 (aryl-C), 116.6 (aryl-C), 121.3 (aryl-C), 132.5 (aryl-C), 141.8 (aryl-C), 146.3 (aryl-C), 149.4 (aryl-C), 159.0 (aryl-C) ppm. UV/Vis: λ_{max} (ϵ) = 326 nm (21250 $\text{M}^{-1}\text{cm}^{-1}$).

$[\text{N}_2\text{O}_2^{\text{red}}]\text{Ti}(\text{py})_2$ (1b): Complex **1b** was prepared by a procedure analogous to that used to prepare **1a**, starting from $\text{TiCl}_4(\text{py})_2$ (0.672 g, 1.93 mmol) and $[\text{N}_2\text{O}_2^{\text{red}}]\text{Li}_4$ (1.93 mmol) in diethyl ether (10 mL). The product was obtained in 79% yield (1.1 g) as purple crystals. X-ray quality crystals were obtained by chilling saturated diethyl ether solutions of the complex to -35 °C. ^1H NMR (600 MHz, C_6D_6): δ = 1.34 [s, 18 H, $\text{C}(\text{CH}_3)_3$], 1.48 [s, 18 H, $\text{C}(\text{CH}_3)_3$], 6.33 (t, $^3J_{\text{HH}} = 6.5$ Hz, 4 H, py), 6.59 (t, $^3J_{\text{HH}} = 7.5$ Hz, 2 H, py), 6.70 (dd, $^3J_{\text{HH}} = 6.9$ and 4.5 Hz, 2 H, aryl-H), 7.07 (d, 2 H, aryl-H), 7.32 (dd, $^3J_{\text{HH}} = 6.9$ and 4.5 Hz, 2 H, aryl-H), 7.38 (d, 2 H, aryl-H), 9.17 (d, $^3J_{\text{HH}} = 5.0$ Hz, 4 H, py) ppm. ^{13}C NMR (125.8 MHz, C_6D_6): δ = 29.8 [$\text{C}(\text{CH}_3)_3$], 31.8 [$\text{C}(\text{CH}_3)_3$], 34.5 [$\text{C}(\text{CH}_3)_3$], 108.7 (aryl-C), 109.0 (aryl-C), 116.6 (aryl-C), 121.2 (aryl-C), 124.3 (py-C), 132.9 (aryl-C), 138.3 (py-C), 141.3 (aryl-C), 144.8 (aryl-C), 147.7 (py-C), 149.1 (aryl-C) ppm. UV/Vis: λ_{max} (ϵ) = 324 nm (33440 $\text{M}^{-1}\text{cm}^{-1}$).

$[\text{N}_2\text{O}_2^{\text{red}}]\text{Zr}(\text{thf})_3$ (2): Complex **2** was prepared by a procedure analogous to that used to prepare **1a**, starting with $\text{ZrCl}_4(\text{thf})_2$ (0.46 g, 1.93 mmol) and $[\text{N}_2\text{O}_2^{\text{red}}]\text{Li}_4$ (1.93 mmol) in diethyl ether (10 mL), containing a few drops of thf. The product was obtained in 55% yield (0.26 g) as yellow crystals. X-ray quality crystals were obtained by chilling saturated diethyl ether solutions of the complex to -35 °C. $\text{C}_{46}\text{H}_{68}\text{N}_2\text{O}_5\text{Zr}$ (820.24): calcd. C 67.36, H 8.36, N 3.42; found C 67.42, H 8.39, N 3.20. ^1H NMR (600 MHz, C_6D_6): δ = 0.87 (s, 12 H, thf), 1.50 [s, 18 H, $\text{C}(\text{CH}_3)_3$], 1.67 [s, 18 H, $\text{C}(\text{CH}_3)_3$], 3.81 (s, 12 H, thf), 6.98 (dd, $^3J_{\text{HH}} = 6.6$ and 3.6 Hz, 2 H, aryl-H), 7.08 (d, $^3J_{\text{HH}} = 2.4$ Hz, 2 H, aryl-H), 7.83 (dd, $^3J_{\text{HH}} =$

6.6 and 3.6 Hz, 2 H, aryl-H), 7.93 (d, $^3J_{\text{HH}} = 4.2$ Hz, 2 H, aryl-H) ppm. ^{13}C NMR (125.8 MHz, C_6D_6): δ = 30.4 [$\text{C}(\text{CH}_3)_3$], 32.5 [$\text{C}(\text{CH}_3)_3$], 34.9 [$\text{C}(\text{CH}_3)_3$], 109.4 (aryl-C), 109.7 (aryl-C), 113.3 (aryl-C), 118.8 (aryl-C), 132.2 (aryl-C), 139.2 (aryl-C), 145.5 (aryl-C), 147.2 (aryl-C), 156.3 (aryl-C). UV/Vis: λ_{max} (ϵ) = 333 nm (15248 $\text{M}^{-1}\text{cm}^{-1}$).

$[\text{N}_2\text{O}_2^{\text{red}}]\text{Hf}(\text{thf})_3$ (3): Complex **3** was prepared by a procedure analogous to that used to prepare **1a**, starting with $\text{ZrCl}_4(\text{thf})_2$ (0.90 g, 1.93 mmol) and $[\text{N}_2\text{O}_2^{\text{red}}]\text{Li}_4$ (1.93 mmol) in diethyl ether (10 mL), containing a few drops of thf. The product was obtained in 57% yield (0.80 g) as yellow crystals. X-ray quality crystals were obtained by chilling saturated diethyl ether solutions of the complex to -35 °C. $\text{C}_{46}\text{H}_{68}\text{N}_2\text{O}_5\text{Hf}$ (907.52): calcd. C 60.88, H 7.55, N 3.09; found C 60.24, H 7.93, N 3.02. ^1H NMR (600 MHz, C_6D_6): δ = 0.79 (s, 12 H, thf), 1.53 [s, 18 H, $\text{C}(\text{CH}_3)_3$], 1.69 [s, 18 H, $\text{C}(\text{CH}_3)_3$], 3.77 (s, 12 H, thf), 7.02 (dd, $^3J_{\text{HH}} = 7.2$ and 4.2 Hz, 2 H, aryl-H), 7.10 (d, $^3J_{\text{HH}} = 2.4$ Hz, 2 H, aryl-H), 7.92 (d, $^3J_{\text{HH}} = 4.2$ Hz, 2 H, aryl-H), 8.02 (dd, $^3J_{\text{HH}} = 7.2$ and 4.2 Hz, 2 H, aryl-H) ppm. ^{13}C NMR (125.8 MHz, C_6D_6): δ = 24.9 (thf), 30.2 [$\text{C}(\text{CH}_3)_3$], 32.2 [$\text{C}(\text{CH}_3)_3$], 34.5 [$\text{C}(\text{CH}_3)_3$], 34.6 [$\text{C}(\text{CH}_3)_3$], 74.2 (thf), 109.9 (aryl-C), 110.2 (aryl-C), 112.6 (aryl-C), 118.2 (aryl-C), 132.6 (aryl-C), 138.8 (aryl-C), 144.9 (aryl-C), 146.6 (aryl-C), 155.7 (aryl-C) ppm. UV/Vis: λ_{max} (ϵ) = 328 nm (8740 $\text{M}^{-1}\text{cm}^{-1}$).

$[\text{N}_2\text{O}_2^{\text{ox}}]\text{TiCl}_2$ (4a): Complex **1a** (0.30 g, 0.43 mmol) was dissolved in diethyl ether (5 mL). The solution was frozen in a liquid nitrogen cold well, and immediately upon melting, freshly-prepared PhICl_2 (0.117 g, 0.43 mmol) was added as a solid. The solution was shaken until all the PhICl_2 had dissolved (2–3 min). The solution color changed from yellow to dark green. A dark-green precipitate began forming, and the mixture was stored at -35 °C. If the reaction mixture warms to room temperature, the yield decreases significantly. After 12 h at -35 °C, the cold solution was filtered to afford **5a** as a dark-green, microcrystalline solid (210 mg, 67% yield). X-ray quality crystals were obtained by slow concentration of a saturated diethyl ether solution of the complex. ^1H NMR (600 MHz, C_6D_6): δ = 1.23 [s, 18 H, $\text{C}(\text{CH}_3)_3$], 1.55 [s, 18 H, $\text{C}(\text{CH}_3)_3$], 6.52 (dd, $^3J_{\text{HH}} = 9.0$ and 3.6 Hz, 2 H, aryl-H), 7.59 (d, 2 H, aryl-H), 7.61 (dd, $^3J_{\text{HH}} = 9.0$ and 3.6 Hz, 2 H, aryl-H), 7.63 (d, $^3J_{\text{HH}} = 9.6$ Hz, 2 H, aryl-H) ppm. UV/Vis: λ_{max} (ϵ) = 948 nm (13172 $\text{M}^{-1}\text{cm}^{-1}$), 427 (15161).

$[\text{N}_2\text{O}_2^{\text{ox}}]\text{TiCl}_2(\text{py})$ (4b): Complex **4b** was prepared by a procedure analogous to that used to prepare **4a**, starting from **1b** (0.40 g, 0.56 mmol) and PhICl_2 (0.134 g, 0.49 mmol) in diethyl ether (5 mL). The product was obtained in 53% yield (210 mg) as dark green crystals. $\text{C}_{39}\text{H}_{49}\text{N}_3\text{O}_2\text{Cl}_2\text{Ti}$ (710.58): calcd. C 65.92, H 6.95, N 5.91; found C 65.82, H 7.26, N 5.65. ^1H NMR (600 MHz, C_6D_6): δ = 1.29 [s, 18 H, $\text{C}(\text{CH}_3)_3$], 1.36 [s, 18 H, $\text{C}(\text{CH}_3)_3$], 6.62 (dd, 2 H, aryl-H, $^3J_{\text{HH}} = 7.0$ and 3.0 Hz), 6.78 (t, 2 H, py, $^3J_{\text{HH}} = 8.4$ Hz), 7.06 (t, 2 H, py, $^3J_{\text{HH}} = 9.6$ Hz), 7.64 (s, 2 H, aryl-H), 7.72 (s, 2 H, aryl-H), 7.78 (dd, 2 H, aryl-H, $^3J_{\text{HH}} = 7.0$ and 3.0 Hz), 9.80 (d, 2 H, py, $^3J_{\text{HH}} = 6.0$ Hz) ppm. ^{13}C NMR (150 MHz, C_6D_6): δ = 29.4 [$\text{C}(\text{CH}_3)_3$], 30.9 [$\text{C}(\text{CH}_3)_3$], 110.0 (aryl-C), 114.3 (aryl-C), 121.1 (aryl-C), 123.8 (aryl-C), 131.5 (aryl-C), 136.7 (py), 138.0 (py), 141.8 (aryl-C), 147.1 (aryl-C), 150.0 (aryl-C), 150.3 (aryl-C) ppm. UV/Vis: λ_{max} (ϵ) = 948 nm (15480 $\text{M}^{-1}\text{cm}^{-1}$), 426 (17569).

$[\text{N}_2\text{O}_2^{\text{ox}}]\text{ZrCl}_2(\text{thf})_2$ (5): Complex **5** was prepared by a procedure analogous to that used to prepare **4a**, starting from **2** (0.40 g, 0.49 mmol) and PhICl_2 (0.134 g, 0.49 mmol) in diethyl ether (8 mL). The product was obtained in 42% yield (153 mg) as dark-green crystals. $\text{C}_{38}\text{H}_{52}\text{N}_2\text{O}_3\text{Cl}_2\text{Zr}$ (746.94): calcd. C 61.10, H 7.02, N 3.75; found C 60.87, H 7.56, N 3.68. ^1H NMR (600 MHz, C_6D_6): δ = 1.32 [s, 18 H, $\text{C}(\text{CH}_3)_3$], 1.64 (br. s, 4 H, thf), 1.70 [s, 18 H,

$C(CH_3)_3$, 4.79 (br. s, 4 H, thf), 6.35 (dd, $^3J_{HH} = 9.0$ and 3.6 Hz, 2 H, aryl-H), 7.52 (dd, $^3J_{HH} = 9.0$ and 3.6 Hz, 2 H, aryl-H), 7.63 (s, 2 H, aryl-H), 7.68 (s, 2 H, aryl-H) ppm. ^{13}C NMR (125.8 MHz, $[D_8]thf$): $\delta = 27.3 [C(CH_3)_3]$, 31.0 $[C(CH_3)_3]$, 32.5 $[C(CH_3)_3]$, 117.7 (aryl-C), 124.9 (aryl-C), 129.5 (aryl-C), 129.9 (aryl-C), 134.5 (aryl-C), 141.0 (aryl-C), 143.1 (aryl-C), 145.9 (aryl-C), 153.8 (aryl-C) ppm. UV/Vis: $\lambda_{max} (\epsilon) = 938$ nm (19718 $M^{-1} cm^{-1}$).

$[N_2O_2^{red}]HfCl_2(thf)$ (6): Complex **6** was prepared by a procedure analogous to that used to prepare **4a**, starting from **3** (0.35 g, 0.39 mmol) and $PhICl_2$ (0.109 g, 0.39 mmol) in diethyl ether (15 mL). The product was obtained in 66% yield (220 mg) as dark-green crystals. $C_{38}H_{52}N_2O_3Cl_2Hf$ (834.22): calcd. C 54.71, H 6.28, N 3.36; found C 54.87, H 6.56, N 3.08. 1H NMR (600 MHz, C_6D_6): $\delta = 1.31$ [s, 18 H, $C(CH_3)_3$], 1.59 (s, 4 H, thf), 1.69 [s, 18 H, $C(CH_3)_3$], 4.75 (s, 4 H, thf), 6.34 (dd, $^3J_{HH} = 9.0$ and 4.2 Hz, 2 H, aryl-H), 7.49 (dd, $^3J_{HH} = 9.0$ and 4.2 Hz, 2 H, aryl-H), 7.61 (s, 2 H, aryl-H), 7.69 (s, 2 H, aryl-H) ppm. ^{13}C NMR (125.8 MHz, $[D_8]thf$): $\delta = 25.3$ (thf), 29.7 $[C(CH_3)_3]$, 31.1 $[C(CH_3)_3]$, 34.6 $[C(CH_3)_3]$, 35.2 $[C(CH_3)_3]$, 74.2 (thf), 116.2 (aryl-C), 123.2 (aryl-C), 131.6 (aryl-C), 140.4 (aryl-C), 141.6 (aryl-C), 143.8 (aryl-C), 152.1 (aryl-C), 168.2 (aryl-C) ppm. UV/Vis: $\lambda_{max} (\epsilon) = 938$ nm (24999 $M^{-1} cm^{-1}$).

Crystal-Structure Analyses: X-ray diffraction data were collected on crystals mounted on glass fibers by using a Bruker CCD platform diffractometer, equipped with a CCD detector. Measurements were carried out at 163 K by using Mo- K_α ($\lambda = 0.71073$ Å) radiation, which was wavelength-selected with a single-crystal graphite monochromator. The SMART program package was used to determine unit-cell parameters and to collect data.^[17] The raw frame data were processed by using SAINT^[18] and SADABS^[19] to yield the reflection data files. Subsequent calculations were carried out by using the SHELXTL^[20] program suite. Structures were solved by direct methods and refined on F^2 by full-matrix least-squares techniques. Analytical scattering factors for neutral atoms were used throughout the analyses.^[21] Hydrogen atoms were included by using a riding model. ORTEP diagrams were generated by using ORTEP-3 for Windows.^[22] CCDC-703149 (**1b**-Et₂O), CCDC-703148 (**3**), and CCDC-703150 (**4a**-C₆H₆) contain the supplementary crystallographic data for this paper. These data can be obtained free of charge from The Cambridge Crystallographic Data Centre via www.ccdc.cam.ac.uk/data_request/cif.

$[N_2O_2^{red}]Ti(py)_2 \cdot Et_2O$ (1b**-Et₂O):** A complete sphere of diffraction data was collected on a yellow crystal of approximate dimensions $0.02 \times 0.28 \times 0.30$ mm by using a 35 s/frame scan time. The diffraction symmetry was $2/m$, and the systematic absences were consistent with the centrosymmetric monoclinic space group $P2_1/m$, which was later determined to be correct. There was one molecule of diethyl ether solvent present per formula unit. Hydrogen atoms were included by using a riding model. Least-squares analysis yielded $wR_2 = 0.1254$ and $Goof = 1.019$ for 505 variables refined against 8494 data (0.82 Å), $R_1 = 0.0496$ for those 5417 data with $I \geq 2\sigma_I$.

$[N_2O_2^{red}]Hf(thf)_3$ (3**):** A complete sphere of diffraction data was collected on a colorless crystal by using a 25 s/frame scan time. The diffraction symmetry was $2/m$, and the systematic absences were consistent with the centrosymmetric monoclinic space group $P2_1/c$, which was later determined to be correct. Hydrogen atoms were included by using a riding model. Least-squares analysis yielded $wR_2 = 0.1661$ and $Goof = 1.075$ for 433 variables refined against 6637 data (0.90 Å), $R_1 = 0.0555$ for those 4530 data with $I \geq 2\sigma_I$.

$[N_2O_2^{ox}]TiCl_2 \cdot C_6H_6$ (4a**-C₆H₆):** A complete sphere of diffraction data was collected on a purple crystal of approximate dimensions $0.07 \times 0.12 \times 0.21$ mm by using a 45 s/frame scan time. The diffrac-

tion symmetry was $2/m$, and the systematic absences were consistent with the centrosymmetric monoclinic space groups Cc and $C2/c$. It was later determined that the centrosymmetric space group $C2/c$ was correct. The molecule was located on a twofold rotation axis, and there was a molecule of benzene solvent present that was located about an inversion center. Hydrogen atoms were located from a difference-Fourier map and refined (x , y , z and U_{iso}). Least-squares analysis yielded $wR_2 = 0.1662$ and $Goof = 1.020$ for 314 variables refined against 3127 data (0.85 Å), $R_1 = 0.0579$ for those 2160 data with $I \geq 2\sigma_I$.

Acknowledgments

Financial support was received from the National Science Foundation (NSF-CAREER, CHE-0645685). A. F. H. is an Alfred P. Sloan Foundation Research Fellow.

- [1] a) C. A. Tyson, A. E. Martell, *J. Am. Chem. Soc.* **1972**, *94*, 939–945; b) M. E. Cass, D. L. Greene, R. M. Buchanan, C. G. Pierpont, *J. Am. Chem. Soc.* **1983**, *105*, 2680–2686; c) M. E. Cass, C. G. Pierpont, *Inorg. Chem.* **1986**, *25*, 122–123; d) C. M. Liu, E. Nordlander, D. Schmeh, R. Shoemaker, C. G. Pierpont, *Inorg. Chem.* **2004**, *43*, 2114–2124; e) C. J. Rolle, K. I. Hardcastle, J. D. Soper, *Inorg. Chem.* **2008**, *47*, 1892–1894.
- [2] C. Stanciu, M. E. Jones, P. E. Fanwick, M. M. Abu-Omar, *J. Am. Chem. Soc.* **2007**, *129*, 12400–12401.
- [3] M. R. Ringenberg, S. L. Kokatam, Z. M. Heiden, T. B. Rauchfuss, *J. Am. Chem. Soc.* **2008**, *130*, 788–789.
- [4] a) S. C. Bart, E. B. Lobkovsky, P. J. Chirik, *J. Am. Chem. Soc.* **2004**, *126*, 13794–13807; b) S. C. Bart, K. Chłopek, E. Bill, M. W. Bouwkamp, E. B. Lobkovsky, F. Neese, K. Wieghardt, P. J. Chirik, *J. Am. Chem. Soc.* **2006**, *128*, 13901–13912; c) S. C. Bart, E. B. Lobkovsky, E. Bill, K. Wieghardt, P. J. Chirik, *Inorg. Chem.* **2008**, *46*, 7055–7063.
- [5] R. A. Zarkesh, J. W. Ziller, A. F. Heyduk, *Angew. Chem. Int. Ed.* **2008**, *47*, 4715–4718.
- [6] K. J. Blackmore, J. W. Ziller, A. F. Heyduk, *Inorg. Chem.* **2005**, *44*, 5559–5561.
- [7] M. R. Haneline, A. F. Heyduk, *J. Am. Chem. Soc.* **2006**, *128*, 8410–8411.
- [8] P. Chaudhuri, M. Hess, J. Müller, K. Hildenbrand, E. Bill, T. Weyhermüller, K. Wieghardt, *J. Am. Chem. Soc.* **1999**, *121*, 9599–9610.
- [9] Portions of this work have been previously reported, see: K. J. Blackmore, N. Lal, J. W. Ziller, A. F. Heyduk, *J. Am. Chem. Soc.* **2008**, *130*, 2728–2729.
- [10] K. J. Blackmore, M. B. Sly, M. R. Haneline, J. W. Ziller, A. F. Heyduk, *Inorg. Chem.*, in press.
- [11] a) P. Chaudhuri, C. N. Verani, E. Bill, E. Bothe, T. Weyhermüller, K. Wieghardt, *J. Am. Chem. Soc.* **2001**, *123*, 2213–2223; b) H. Chun, C. N. Verani, P. Chaudhuri, E. Bothe, E. Bill, T. Weyhermüller, K. Wieghardt, *Inorg. Chem.* **2001**, *40*, 4157–4166; c) S. Bhattacharaya, P. Gupta, F. Basuli, C. G. Pierpont, *Inorg. Chem.* **2002**, *41*, 5810–5816.
- [12] a) C. G. Pierpont, *Coord. Chem. Rev.* **2001**, *216–217*, 99–125; b) D. N. Hendrickson, C. G. Pierpont, *Top. Curr. Chem.* **2004**, *234*, 63–95.
- [13] a) C. Floriani, E. Solari, F. Corazza, A. Chiesivilla, C. Guastini, *Angew. Chem. Int. Ed. Engl.* **1989**, *28*, 64–66; b) V. I. Tararov, D. E. Hibbs, M. B. Hursthouse, N. S. Ikonnikov, K. M. A. Malik, M. North, C. Orizu, Y. N. Belokon, *Chem. Commun.* **1998**, 387–388; c) H. Y. Chen, P. S. White, M. R. Gagné, *Organometallics* **1998**, *17*, 5358–5366.
- [14] F. Corazza, E. Solari, C. Floriani, A. Chiesivilla, C. Guastini, *J. Chem. Soc., Dalton Trans.* **1990**, 1335–1344.
- [15] L. E. Manzer, *Inorg. Synth.* **1982**, *21*, 135–140.
- [16] H. J. Lucas, E. R. Kennedy, *Org. Synth.* **1955**, *3*, 482.

- [17] *SMART Software Users Guide*, Version 5.1, Bruker Analytical X-ray Systems, Inc., Madison, WI, **1999**.
- [18] *SAINT Software Users Guide*, Version 6.0, Bruker Analytical X-ray Systems, Inc., Madison, WI, **1999**.
- [19] G. M. Sheldrick, *SADABS*, Version 2.10, Bruker Analytical X-ray Systems, Inc., Madison, WI, **2002**.
- [20] G. M. Sheldrick, *SHELXTL*, Version 6.12, Bruker Analytical X-ray Systems, Inc., Madison, WI, **2001**.
- [21] *International Tables for X-ray Crystallography*, Kluwer Academic Publishers, Dordrecht, **1992**, vol. C.
- [22] L. J. Farrugia, *J. Appl. Crystallogr.* **1997**, 30, 565.

Received: September 23, 2008
Published Online: January 20, 2009